Fast circular shapes detection in cylindrical ECT sensors by design selection and nonlinear black-box modeling

Yacine Oussar, Cedric Margo, Jérôme Lucas, Stéphane Holé

Fast circular shapes detection in cylindrical ECT sensors by design selection and nonlinear black-box modeling

Yacine Oussar (LPEM, ESPCI Paris, PSL Research University, Sorbonne Universités, UPMC Univ Paris 06, CNRS, Paris, France)
Cedric Margo (LPEM, ESPCI Paris, PSL Research University, Sorbonne Universités, UPMC Univ Paris 06, CNRS, Paris, France)
Jérôme Lucas (LPEM, ESPCI Paris, PSL Research University, Sorbonne Universités, UPMC Univ Paris 06, CNRS, Paris, France)
Stéphane Holé (LPEM, ESPCI Paris, PSL Research University, Sorbonne Universités, UPMC Univ Paris 06, CNRS, Paris, France)

September 8, 2016

Abstract

Purpose - Within the framework of image reconstruction in cylindrical Electrical Capacitance Tomography (ECT) sensors, a sensor structure is selected, in terms of number and size of the electrodes, to predict the radius and the position of a single circular shape lying in the cross-section defined by the sensor electrodes.

Design/methodology/approach - Nonlinear black-box models using a set of physically independent capacitances and Least-Square Support Vector Machines (LS-SVM) models selected with a sophisticated validation method are implemented.

Findings

- The coordinates of circular shapes are well estimated in fixed and variable permittivity environments even with noisy data. Various numerical experiments are presented and discussed. Sensors formed by 3 or 4 electrodes covering 50% of the sensor perimeter provide the best prediction performances.

Research limitations/implications

- The proposed method is limited to detect a single circular shape in a cylindrical ECT sensor.

Practical implications

- This method can be advantageously implemented in real time applications since it is numerically cost effective and necessitates a small amount of measurements.

Originality/value

- The contribution is twofold: (i) a fast computation of a circular shape position and radius with a satisfactory precision compared to the sensor size, (ii) the determination of a cylindrical ECT sensor architecture that allows the most efficient predictions.

1 Introduction

Electrical Capacitance Tomography (ECT) is a well-known and a widely used sensing technique (Yang 2010). Generally, an ECT sensor is formed by a set of electrodes arranged circularly. The sensing technique consists in measuring the electrical capacitances between all possible couples of electrodes. Typically, an ECT sensor can yield information on the spatial configuration (size, position) of a non-conducting material whose permittivity is different from that of the environment. Such situation is common when gas bubbles appear in a fluid conveyed in a pipe.

The cross-sectional image of the sensed area of interest can be obtained using capacitance measurements. Usually, the pixels correspond to nodes from a spatial discretization scheme that involves a linear knowledge-based model. This model describes the relationship between the measurements and the permittivity at each node. The image resolution increases with the space discretization. Constructing the image leads to invert an underdetermined set of linear equations (Yang & Peng 2003).

The literature dedicated to ECT sensors presents various applications: corn moisture measurement, imaging in fluids, flow measurement. While both the number and the size of electrodes have great importance regarding the sensor performances, they are usually set arbitrarily and seldom discussed (Chen, Hu, Liu & Xuang Gao 2011). In addition, in most of the studies, all the physically independent measurements are used (Wang & Zhang 2009). One can wonder if they are all relevant or just a few of them are sufficient to achieve the best image reconstruction given the sensor structure. Moreover, one might ask: what should be a good structure of the sensor for a given application?

The present study focuses on structure selection (number and size of electrodes) in cylindrical ECT sensors that permits a fast detection of circular shapes with sufficient accuracy. In this work, it is assumed that tuning the number and the size of electrodes allows to optimize the sensor performances for a given application. More precisely, the goal consists in determining the sensor architecture that best predicts the size and the position of a single circular shape in the sensor cross-section. Two different situations are considered. In the first one, the environment permittivity is fixed. In the second one, the environment permittivity can take any value in a known domain. To achieve this goal, non linear black box models were implemented using Least-Square Support Vector Machines (LS-SVM) to establish the relationship between the measured capacitances and the circular shape in terms of size and position.

The paper is organized as follows: Section 2 recalls briefly the ECT sensors background and states the problem. Section 3 describes the LS-SVM modeling technique and the validation method implemented in this work. Section 4 is dedicated to data generation. Sections 5 and 7 present the selection of the most efficient design of ECT sensors, among those considered, in respectively, fixed permittivity and variable permittivity environments. Section 6 illustrates the impact of noisy measurements on the sensor structure that achieves the best prediction performance.

2 ECT sensor and problem statement

2.1 Brief recall of ECT sensor background

Figure 1 illustrates the structure of a typical ECT sensor considered in this study. It is formed by a set of guarded electrodes arranged circularly. The electrodes consist for instance of two conducting layers separated by an insulator. The internal layer is the measurement electrode on which the charges are measured. The external layer is always driven with the same potential as the measurement electrode but the charges it holds are not measured. As long as the external electrode and the insulating layer are sufficiently thin, the field inside the sensor is little modified. Since the the potentials are the same on both the guard and the electrode, the field between them is null. Consequently, the insulting layer does not contribute to the signal. Due to the circular symmetry of the sensor, the guard electrodes insure that the electrical field originating from the measurement electrodes is restricted to the closed region circumscribed by the sensor electrodes. Finally, the designed ECT sensor is only sensitive to its inside region.

The environment delimited by the sensor is characterized by a permittivity ε_1. A non conducting single circular shape with permittivity ε_2 lies inside the sensor . This circular shape has unknown size and position respectively pointed by a radius R and two coordinates: x and y. According to this formulation, the image reconstruction consists in estimating as accurately as possible the radius and the coordinates of the circular shape.

The measurement of the capacitances appearing between the sensor electrodes are performed by polarizing each electrode independently. When a potential V_j is applied to electrode j while all the other electrodes are grounded, the measurement of the charge Q_i appearing on electrode i allows the capacitive

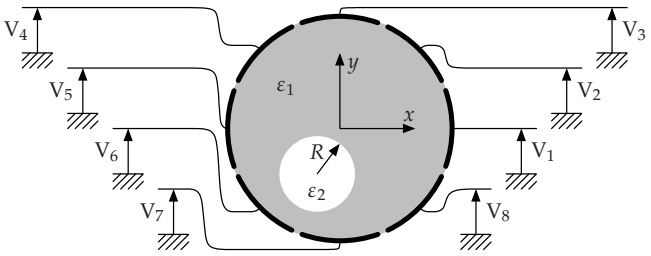

Figure 1: An 8-electrode ECT sensor

tensor c_{ij} to be determined according to the relation:

$$Q_i = c_{ij} V_j \tag{1}$$

For a given P-electrode sensor, the complete capacitive sensor c_{ij} can be expressed using the capacitances C_{ij} connecting electrode i to electrode j as follows:

$$c_{ij} = \begin{bmatrix} \sum_j C_{1j} & -C_{12} & -C_{13} & \cdots & -C_{1P} \\ -C_{12} & \sum_j C_{2j} & -C_{23} & \cdots & -C_{2P} \\ -C_{13} & -C_{23} & \sum_j C_{3j} & \cdots & -C_{3P} \\ \vdots & \vdots & \vdots & \ddots & \vdots \\ -C_{1P} & -C_{2P} & -C_{3P} & \cdots & \sum_j C_{Pj} \end{bmatrix} \tag{2}$$

Since the capacitive sensor is symmetric and the diagonal components are a linear combination of other capacitances, there are at most $\frac{1}{2}P\left(P-1\right)$ independent capacitances where P is the number of electrodes. Usually, the image reconstruction consists in determining the permittivity distribution by solving an underdetermined set of linear equations using an iterative algorithm (Yang & Peng 2003, Jang, Lee, Kim & Choi 2006). The algorithm minimizes a cost function given by:

$$J = \left(m_{ij} - S_{ijk} V \hat{\varepsilon}_k\right)^2 \tag{3}$$

where m_{ij} is the measurement at electrode i when electrode j is under the voltage V while all the other electrodes are grounded. Here m_{ij} is homogeneous to a charge, but it could be a current or a potential. Indeed it was proven that they are all equivalent (Lucas, Holé & C.Batis 2006, Lucas, Holé & Batis 2008). $\hat{\varepsilon}_k$ is the permittivity of a small element k resulting from the spatial discretization of the cross-section of interest. S_{ijk} is the sensor sensitivity matrix. It is usually defined as (Xie, Huang & Hoyle 1992):

$$S_{ijk} = \frac{\delta v^{max}}{\delta v_k} \times \frac{C_{ij}\left(\varepsilon_k = \varepsilon^{max}\right) - C_{ij}\left(\varepsilon_k = \varepsilon^{min}\right)}{\varepsilon^{max} - \varepsilon^{min}} \tag{4}$$

where δv_k is the "volume" of kth element resulting from the spatial discretization of the cross-section and δv^{max} is the "volume" of the largest element. $C_{ij}\left(\varepsilon_k = \varepsilon^{max}\right)$ and $C_{ij}\left(\varepsilon_k = \varepsilon^{min}\right)$ are respectively the capacitances when the permittivity takes its maximum value ε^{max} and its minimum value ε^{min} in the kth element of volume.

Relation 3 assumes that an additive noise acts on the measurement process. It is generally the case for capacitive systems. Thus, if the predictive model is relevant and its parameters properly estimated, the cost function of relation 3 will be equal to the noise variance.

2.2 Problem statement

In the present study, an ECT sensor is fully defined by providing the number and the size of the electrodes. Indeed, this couple along with the circular geometry set the complete sensor structure. While it is assumed that a single circular pattern lies in the sensor, the basic motivation for this study is twofold: (i) lead to the most accurate and computationally cost effective prediction of its size and position, (ii) selecting an efficient sensor architecture regarding the assigned objective.

In Figure 1, the gap between electrodes is relatively small. This may not be always the case since the size and the number of electrodes have a significant impact on the sensor performances. In an ECT sensor such as on Figure 1, the size of electrodes can be deduced from their number and from the ratio of the sensor perimeter they cover. Therefore, for a given covering ratio, studying the influence of the number of electrodes allows to study simultaneously the influence of the size of the electrodes. Thus, the study was performed considering two parameters: the number of electrodes and the covering ratio. However, see for instance (Lucas, Margo, Oussar & Holé 2015) section 3.4, it is relevant to consider three types of electrode size : wire, intermediate and contiguous electrodes.

Figure 2: ECT sensor formed by a set of wire electrodes and dedicated to the measurement of water content in wood-chips.

- Wire electrodes: they cover a small ratio of the sensor perimeter, less than 10% typically. They were successfully used by the authors for the design of ECT sensors dedicated to the measurement of water content in wood-chips (Cuvigny, Bourdil, Géron, Lucas, Ditchi & Holé 2010, Margo, Lucas, Ditchi, Géron, Holé & Lewiner 2011). Figure 2 shows an ECT sensor whose electrodes cover 6% of the perimeter. It is connected to an electronic device that carries out charge measurements.
- Intermediate electrodes: they cover any other ratio of the sensor perimeter. Three values are considered in this study: 25%, 50% and 75%.
- Contiguous electrodes: they cover the major sensor perimeter, more than 90%.

Figure 3 illustrates these three types of ECT sensors.

Instead of dealing with an image reconstruction founded on inverting an underdetermined set of equations by minimizing the cost function given by relation 3, a black-box inverse model that predicts the size and the position of single circular pattern is preferred and can be designed using data generated by numerical experiments. The black-box models are implemented using the LS-SVM technique. Since the output of a LS-SVM model is computed using a set of basic arithmetic operations, this approach allows an almost instantaneous prediction of the pattern configuration which makes it highly attractive for a real-time implementation.

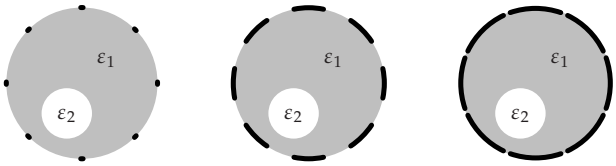

Figure 3: ECT sensors with wire electrodes (left), intermediate electrodes (middle) and contiguous electrodes (right)

3 Training and validating LS-SVM models

3.1 LS-SVM model description

In spite of several and efficient techniques for non linear static modeling, such as neural networks, Least Square Support Vector Machines (LS-SVM) are attractive candidates thanks to various interesting properties: they are linear-in-their-parameters models, their training algorithm consists in a quadratic minimization and they have a built-in regularization mechanism (Vapnik 1995). As a result, these properties confer to them the ability to build models with high generalization capabilities by avoiding overfitting and controlling model complexity. Given a set D formed by N examples of S variables and a scalar z: $D = \left\{(\mathbf{t}_i, z_i) \in \mathbb{R}^S \times \mathbb{R},\ i = 1, ...N\right\}$, nonlinear models of the form:

$$\hat{z} = \mathbf{w}^T \varphi(\mathbf{t}) + b \tag{5}$$

are implemented, where $\mathbf{t}$ is the vector of input variables, $\hat{z}$ is the model output, $\mathbf{w}$ and b are unknown parameters and function φ, usually introduced by a kernel function, is a nonlinear mapping from the original feature space to a higher dimensional feature space (Cristianini & Shawe-Taylor 2000). The LS-SVM training procedure consists in minimizing the cost function defined by:

$$J(\mathbf{w}, \mathbf{e}) = \frac{1}{2}\|\mathbf{w}\|^2 + C\sum_{i=1}^{N} e_i^2 \tag{6}$$

subject to the equality constraints $e_i = z_i - \hat{z}_i$ with e_i the prediction error taking into account the target output z_i and the predicted output $\hat{z}_i$. N is the size of the training set and C is the regularization parameter. This optimization problem can be cast into a dual form with unknown parameters $\boldsymbol{\alpha}$ and b, $\boldsymbol{\alpha}$ being the vector of the Lagrange multipliers (Bertsekas 1999). The parameters can be computed by resolving the following set of linear equations:

$$\underbrace{\begin{bmatrix} \mathbf{K} + \frac{1}{2C}\mathbf{I_N} & \mathbf{1}_N \\ \mathbf{1}_N^T & 0 \end{bmatrix}}_{\text{matrix } \mathbf{M}} \begin{bmatrix} \boldsymbol{\alpha} \\ b \end{bmatrix} = \begin{bmatrix} \mathbf{z} \\ 0 \end{bmatrix} \tag{7}$$

with $\mathbf{1}_N = [1, 1, ..., 1]^T$, $\boldsymbol{\alpha} = [\alpha_1, \alpha_2, ..., \alpha_N]^T$ and $\mathbf{I_N}$ is the identity matrix. K is the kernel matrix: its component k_{ij} is defined as the dot product between the $\varphi(\mathbf{t}_i)$ and the $\varphi(\mathbf{t}_j)$ mappings. In our study, the Gaussian kernel is used. It is a common choice when practicing non linear modeling with SVM. It introduces an additional parameter σ which is its standard deviation. The expression of k_{ij} is given by:

$$k_{ij} = K(\mathbf{t}_i, \mathbf{t}_j) = \exp\left(-\frac{\left\|\mathbf{t}_i - \mathbf{t}_j\right\|^2}{\sigma^2}\right) \tag{8}$$

Parameters σ and C are called the hyperparameters of the LS-SVM model. Their values can be opti-

mized using a validation procedure. Hence, the expression of the model becomes:

$$\hat{z} = \sum_{i=1}^{N} \alpha_i \mathbf{K}\left(\mathbf{t}_i, \mathbf{t}\right) + b \tag{9}$$

where $\boldsymbol{\alpha}$ and b are the solutions of the system given by (7).

3.2 LS-SVM model selection procedure

Since LS-SVM models are linear in their parameters models, the solution of the training phase is unique and can be computed straightforwardly using the set of linear equations given by relation (7). This holds when the hyperparameters C and σ are known with fixed values. Usually, these hyperparameters are unknown and must be computed prior to the training phase. A suitable way to proceed consists in selecting the couple (C, σ) that best validates the LS-SVM model. In practice, the generalization capabilities of such black box model are estimated by computing the validation error. Various validation techniques exist in the literature (Hastie, Tibshirani & Friedman 2009). The most popular technique is probably the cross validation method and the Leave-One-Out (LOO) technique. Since a fine search is desirable to best optimize the model performance, the computational burden can rapidly become untractable when using either methods. In order to reduce substantially the computational time of the selection procedure without compromising its efficiency, the validation error is estimated using the Virtual Leave-One-Out (VLOO) method. This method, first proposed for linear models (Belsley, Kuh & Welsh 1980) and later extended to nonlinear models (Laurent & Cook 1993), allows an estimation of the validation error to be computed by performing only one training involving the whole available data. This estimation is exact when dealing with linear-in-their-parameters models, such as LS-SVM models, while it remains an approximation for models which are non-linear with respect to their parameters. More recently, a framework was described (Cawley & Talbot 2007) to implement the VLOO method for LS-SVM models. For a given LS-SVM model, the VLOO error is computed as:

$$\text{VLOO error} = \sqrt{\frac{1}{N}\sum_{i=1}^{N}\left\{\frac{\alpha_i}{\left(\mathbf{M}^{-1}\right)_{ii}}\right\}^2} \tag{10}$$

where N is the size of the training set, and $\left(\mathbf{M}^{-1}\right)_{ii}$ is the i-th diagonal element of the inverse of matrix $\mathbf{M}$ that appears in relation (7). Thus, the VLOO permits a fast and exact estimation of the validation error which consists in a great benefit when optimizing the values of the hyperparameters according to a grid search.

4 Data generation

As discussed in section 2.2 and presented above, the configuration of a circular shape is predicted using LS-SVM models. These black box models must be trained using data. The data can be generated using either a real experimental setup or numerical experiments. Since a large number of real experiments is complicated to carry out, the study uses data generated by simulations. Indeed, the simulation of electric fields is considered as very efficient. Moreover, it makes it possible to finely study parasitic effects such as noise. Since electrodes are considered of sufficient length compared to the sensor and bubble radii, invariance by translation can be assured. As a consequence, most of the simulations were carried out in 2D.

Following others studies (Yang & Peng 2003, Chen et al. 2011) that use real measurements, it is assumed that the sensor sensitivity is sufficient. Consequently, the generated data can be considered informative and relevant to be used to design black box models with machine learning techniques. Thus, data was generated using a knowledge-based model given by a set of differential equations. The spatial discretization of the sensor is implemented using the finite element modeling approach with Gmsh software (Dular & Geuzaine (accessed November 2011)). The differential equations are solved using GetDP software (Dular & Geuzaine (accessed January 2012)). Figure 4 illustrates the electrical field lines computed by GetDP when a circular form is present in the sensor. The three electrodes are alternately polarized. When an electrode is polarized to 1 V, the 2 others are grounded. Note that guard electrodes considered in our simulations do not appear on Figure 4 since they are held at the same potential as their corresponding measurement electrodes and they can not be distinguished from the measurement ones at the figure scale. This work considers circular forms of air with relative permittivity $\varepsilon_2 = 1$ in an oil flow having a relative permittivity $\varepsilon_1 = 3$. Thus, the field lines appear almost straight in the circular shape since its permittivity is smaller than the environment permittivity. One can also observe that the field lines are exploring the whole area bounded by the sensor. This does not happen consistently. In particular, when the number of electrodes is large and/or the electrodes are contiguous, the field lines stand in the vicinity of the gaps between the electrodes and miss a large part of the domain circumscribed by the sensor.

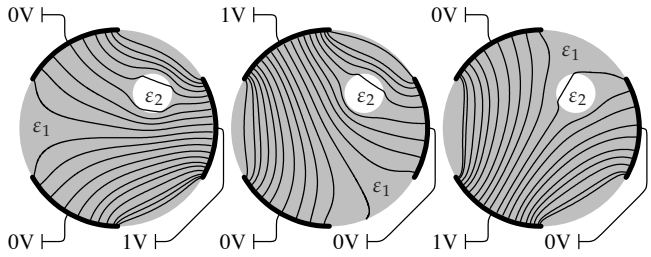

Figure 4: Typical field lines distribution in a 3-electrode sensor in presence of a single circular form. Each time a different electrode is polarized to 1 V while the two others are grounded. For the sake of clarity, only internal field lines are represented.

For a given sensor structure defined by the number of electrodes and their size, 500 to 1000 circular forms with random sizes and positions are generated. Each time a triplet (x, y, R) is drawn from a uniform distribution, it is necessary to check if the shape of the circular form is limited to the closed region circumscribed by the sensor electrodes. If so, the item is selected and the corresponding capacitances calculated. Otherwise, the form does not correspond to a realistic configuration. Thereby, it is rejected. This procedure is iterated until the required number of numerical experiments is reached.

5 Selecting an efficient sensor architecture for a fixed permittivity environment

In this section,the design of ECT sensors with a fixed value of the environment permittivity is considered. Basically, the design of the inverse model is implemented using three independent models: each of them

predicts a component of the triplet (x, y, R) as given by equation (11).

$$\begin{cases} \hat{x} & = \varphi_1(\text{independent measurements}) \\ \hat{y} & = \varphi_2(\text{independent measurements}) \\ \hat{R} & = \varphi_3(\text{independent measurements}) \end{cases} \tag{11}$$

The search of an efficient sensor architecture leads to a combinatorial optimization. A grid search is applied by considering all the sensors with a number of electrodes in {2, 3, 4, 5, 6, 8, 12, 16} and electrode sizes in {1%, 25%, 50%, 75%, 99%}.

A first attempt to build inverse models to predict the configuration of circular shapes with a linear LS-SVM leads to poor generalization capabilities. This result concerns the modeling technique and not the sensor selection. It means that linear modeling is not sufficient to capture the relationship between the measurements and the output variables to be predicted. Therefore, nonlinear models were implemented using the Gaussian kernel.

Figure 5 shows the validation error for the prediction of the radius R (top graph), the coordinates x (middle graph) and y (bottom graph). Obviously, a 2-electrode sensor is not satisfactory to predict the circular shape configuration. With 3 or more electrodes, all the sensors provide enough information to estimate accurately the circular shape size and position with some differences depending on electrodes size.

Regarding coordinates x and y, a more thorough analysis of the results shows that the most accurate model is obtained with 3 electrodes of intermediate size 50%. The VLOO error computed using relation (10) is less than 3% of the sensor radius. Increasing the number of electrodes leads systematically to less efficient models. For intermediate size electrodes, the error increases almost monotonically. However, the behavior of sensors with contiguous electrodes is quite different. At least 5 electrodes are required to achieve a satisfactory prediction accuracy. This can be explained physically by the penetration of the electric field in the sensor. Contrarily to intermediate electrodes, the electric field with contiguous electrodes is indeed concentrated at the junctions between electrodes. Therefore, with contiguous electrodes, increasing their number better distributes the electrical field in the sensor.

Predicting the circular shape size is clearly less critical than the coordinates x and y. A 2-electrode sensor of intermediate size 50% allows to predict radius R with an error of less than 1% of the sensor radius. Similarly to the coordinates, the radius prediction with a contiguous electrodes sensor requires at least 5 electrodes.

The sensors formed by 8, 12 or even 16 electrodes are often preferred in the literature devoted to ECT sensors and show satisfactory performances. However, it appears clearly that such an amount of electrodes is not necessary to estimate efficiently the size and the position of a single circular shape when using the approach proposed in this study.

These promising results were obtained with data obtained with 2D simulations. One can wonder if they are still sound when dealing with data that come from 3D simulations. In order to have a better insight of the effectiveness of the proposed methodology in the 3D case, a set of nonlinear LS-SVM models were built and selected using data that take into account the physical properties of ECT sensors in 3D. ECT sensors formed by 2 to 8 electrodes of intermediate size 50% were considered. Figure 6 shows the best validation errors obtained for the three coordinates. These errors are compared with those obtained with 2D simulations and the same sensor configurations. Predicting the circular shapes coordinates in a 3D configuration comes with larger errors. They are roughly: (i) 2 times larger for coordinates x and

y, (ii) 3 times larger for predicting the radius R. However, these errors remain satisfactory. Coordinates x and y are best predicted by a 3-electrode sensor with errors representing 6.8% and 5.2% of the sensor radius respectively. The estimation of radius R is achieved with an error less then 1% of the sensor radius regardless of the number of electrodes. Thus, it is reasonable to consider that validating the proposed method with 2D simulations is representative of what would be obtained with 3D simulations. Using 2D simulations has also the advantage to be computationally faster.

6 Noise robustness

In the previous experiments, data were noise free. If it were real measurements, data would be impacted by noise. This may lead to a decrease in the prediction performance. Since our aim is to select an efficient design of ECT sensors, one can wonder how does the presence of noise in the data influence the sensor structure that achieves an efficient coordinates estimation.

To study the effect of noise in the measurements, several numerical experiments were conducted. A time varying noise was introduced in a test set as realizations of a uniformly distributed random variable in the interval $[-a, a]$. Six different distributions were considered corresponding to different values of a: 0.1%, 0.3%, 1%, 3%, 10% and 30% of the average signal amplitude.

Figure 7 illustrates the test error for the prediction of radius R (top graph), coordinate x (middle graph) and coordinate y (bottom graph) for all the sensors formed by a number of electrodes in {3, 4, 5, 6, 8, 12, 16} and covering 50% of the sensor perimeter. For the sake of clarity and in order to limit the figure number, this electrode size was preferred since it showed better performances than other sizes as presented in section 5.

The test error for radius R never exceeds 4% of the sensor radius whatever the sensor architecture between 3 and 6 electrodes. Sensors with larger number of electrodes have worse performances. Thus, the prediction of radius R is not much affected by the presence of noise: a 4-electrode sensor provides the best performance whatever the noise amplitude. However, the best sensor architecture for predicting coordinates x and y evolves differently when the noise amplitude increases. Indeed, for a noise amplitude under 3% of the average signal amplitude, a 3-electrode sensor remains the most efficient to predict the circular shape position. With more electrodes, the test error increases. On the contrary, for a noise amplitude of 10% or more, the performance of sensors formed by 3 to 6 electrodes deteriorates drastically. The 8-electrode sensor offers the best compromise. Since beyond 3 electrodes, the information brought by the measurements does not improve the prediction performance, the latest observation indicates that the information redundancy helps to overcome the presence of noise.

7 Selecting an efficient sensor architecture with a variable permittivity environment

In this section, the design of an ECT sensor that can be used with different values of the environment permittivity is studied. Typically, such sensor is helpful when several fluids with different permittivities can be conveyed in the same pipe. Indeed, the performance of the sensors designed according to the method described above decreases drastically when the environment permittivity changes. In our experiments the environment permittivity value ε_1 is known and can take any value in the range from 2 to 4 (Olive Oil, Gasoline, Phenol). The values of ε_1 are uniformly distributed between these two values. The goal

remains the detection of both size and position of circular shapes made of air. Thereby, the circular shapes permittivity value is constant: $\varepsilon_2 = 1$.

When the environment permittivity is fixed, it is not a relevant information to design the models given by equation (11). However, when the environment permittivity is variable, it influences the measurements and then should be a priori taken into account as a relevant input in the design of the nonlinear inverse models as shown by relation (12). Similarly to the previous sections, models of equation (11) are built using the LS-SVM modeling technique. Sets of data were generated for each sensor structure formed by 2 up to 7 electrodes. Indeed, the results presented above show that sensors formed by more than 6 electrodes are oversized to predict the configuration of a single circular form using noise free measurements.

Sets formed by 500 samples failed to train efficiently models that achieve a satisfactory performance in the prediction of the triplet $(\hat{x},\hat{y},\hat{R})$. This means that the relationship between the independent measurements and the variables x, y and R is more complex to model when ε_1 is a variable parameter. As a result, training and validation were conducted using larger sets formed by 1000 examples. The size of the training set was set to 1000 samples since this value ensures good results. Smaller sets formed by 500 to 1000 samples might be sufficient. While the size of the training set can be an important issue when modeling from data, it is out of our concern in this study.

$$\begin{cases} \hat{x} & = \psi_1(\text{independent measurements}, \varepsilon_1) \\ \hat{y} & = \psi_2(\text{independent measurements}, \varepsilon_1) \\ \hat{R} & = \psi_3(\text{independent measurements}, \varepsilon_1) \end{cases} \tag{12}$$

Figure 8 illustrates the validation error for the prediction of radius R (top graph), coordinate x (middle graph) and coordinate y (bottom graph) for all sensors formed by 2 to 7 electrodes. Dark bars correspond to models given by relation (12): ε_1 is an input variable, while white bars correspond to models given by relation (11): ε_1 is not provided to the model as an input variable. For radius R, the prediction error is less than 1% of the sensor radius regardless of the number of electrodes when ε_1 is as an input variable. However, if ε_1 is excluded from the set of input variables, an efficient prediction of R is obtained with sensors formed by 4 electrodes or more. Thus, the redundancy in the information compensates for the lack of input ε_1. The prediction of both coordinates x and y is almost independent of variable ε_1 as an input. However, the redundancy also plays a role here. Indeed, the best validation error is obtained with a 5-electrode sensor while for a fixed permittivity environment, the best performance was obtained with a 3-electrode sensor.

Although coordinates x and y are predicted with an error of 7% against less than 3% when the permittivity environment is fixed, theses results show the ability of the nonlinear modeling to take into account the variation of the permittivity of the environment solely from the measurements of the capacitances.

8 Conclusion

This study is dedicated to the selection of an efficient design in ECT sensors for detecting the size and the position of a single circular shape in both fixed and variable permittivity environment. The influence of both the number and the size of the electrodes were investigated and discussed. To this aim, non linear inverse models involving the LS-SVM technique were implemented. Theses models were validated by an efficient validation procedure. The nonlinear inverse models predict the size and the position of a single circular shape using independent measurements.

Regarding the number of electrodes, our results show that increasing this parameter does not lead systematically to an improvement of the sensor performance. For a fixed permittivity environment, the best accuracy is achieved with a sensor formed by 3 electrodes. For a variable permittivity environment, the best performance is obtained with a 5-electrode sensor. This result is counterintuitive since most of the other studies involve ECT sensors with much more electrodes. In the presence of moderate noise, this result holds. However, when the measurements are very noisy, more electrodes are required to achieve a good performance. An 8-electrode sensor shows the best performance.

Albeit to a lesser extent, the electrode size also has an impact on the sensor performance. In a fixed permittivity environment, the most accurate sensor was obtained using intermediate size electrodes that cover 50% of the sensor perimeter. The overall results show that the sensor performances are roughly stable with wire or intermediate size electrodes (between 25% and 75% of the sensor perimeter). However, the use of contiguous electrodes requires more electrodes to achieve satisfactory performances. Besides, this technique is efficient with circular shapes. Whenever non circular shapes are presented to the predictive models, the results will be irrelevant. In such situation, new models have to be designed with relevant data drawn from either numerical experiments or physical measurements.

The main result of our study: the use of a 3-electrode sensor in a fixed permittivity environment and 5-electrode sensor in a variable permittivity environment, associated to an image reconstruction via a direct calculation for a single circular shape localization and sizing, leads to a computational cost effective sensing approach. This makes it highly attractive for real-time implementations.

References

Belsley, D., Kuh, E. & Welsh, R. (1980), *Regression Diagnostics: Identifying Influential Data And Sources Of Collinearity*, John Wiley and Sons, New York, NY.

Bertsekas, D. P. (1999), *Nonlinear Programming (Second ed.)*, Athena Scientific, Cambridge, MA.

Cawley, G. C. & Talbot, N. L. C. (2007), 'Preventing over-fitting during model selection via bayesian regularization of the hyper-parameters', *JMLR* **8**, 841–861.

Chen, X., Hu, H., Liu, F. & Xuang Gao, X. (2011), 'Image reconstruction for an electrical capacitance tomography system based on a least-squares support vector machine and a self-adaptive particle swarm optimization algorithm', *Measurement Science and Technology* **22**, 1–9.

Cristianini, N. & Shawe-Taylor, J. (2000), *Support Vector Machines and other Kernel-based Learning Methods*, Cambridge University Press, Cambridge, UK.

Cuvigny, N., Bourdil, C., Géron, E., Lucas, J., Ditchi, T. & Holé, S. (2010), 'Measuring the retrievable energy from wood-chips using an electrostatic method', *Proceedings of the 7th Conference of the French Society of Electrostatics* . SFE2010, Montpellier (France).

Dular, P. & Geuzaine, C. ((accessed January 2012)), 'Available online: http://www.geuz.org/getdp/'.

Dular, P. & Geuzaine, C. ((accessed November 2011)), 'Available online: http://geuz.org/gmsh/'.

Hastie, T., Tibshirani, R. & Friedman, J. (2009), *The Elements of Statistical Learning*, Springer, New York, NY.

Jang, J., Lee, S., Kim, K. & Choi, B. (2006), 'Modified iterative landweber method in electrical capacitance tomography', *Measurement Science and Technology* **17**, 1909–1917.

Laurent, R. T. S. & Cook, R. D. (1993), 'Leverage, local influence and curvature in nonlinear regression', *Biometrika* **80**, 99–106.

Lucas, J., Holé, S. & Batis, C. (2008), 'Simple and direct calculation of capacitive sensor sensitivity map', *COMPEL - The International Journal for Computation and Mathematics in Electrical and Electronic Engineering* **27**, 307–318.

Lucas, J., Holé, S. & C.Batis (2006), 'Analytical capacitive sensor sensitivity distribution and applications', *Measurement Science and Technology* **17**, 2467–2478.

Lucas, J., Margo, C., Oussar, Y. & Holé, S. (2015), 'Physical limitations on spatial resolution in electrical capacitance resolution', *Measurement Science and Technology* **26**, 1–12.

Margo, C., Lucas, J., Ditchi, T., Géron, E., Holé, S. & Lewiner, J. (2011), 'Wood-chip water content sensor with capacitive tomography', *Proceedings of the 10th International Symposium of Measurement Technology and Intelligent Instruments* . ISMTII 2011, Daejeon (Korea).

Vapnik, V. (1995), *The Nature of Statistical Learning Theory*, Springer, New York, NY.

Wang, H. X. & Zhang, L. F. (2009), 'Identification of two-phase flow regimes based on support vector machine and electrical capacitance tomography', *Measurement Science and Technology* **20**, 1–8.

Xie, C. G., Huang, S. M. & Hoyle, B. S. (1992), 'Electrical Capacitance Tomography for Flow Imaging: System Model for Developement of Image Reconstruction Algorithms and Design of Primary Sensors', *IEE Proceedings, Vol. 139* .

Yang, W. Q. (2010), 'Design of electrical capacitance tomography sensors', *Measurement Science and Technology* **21**, 225–232.

Yang, W. Q. & Peng, L. (2003), 'Image reconstruction algorithms for electrical capacitance tomography', *Measurement Science and Technology* **14**, R1–R13.

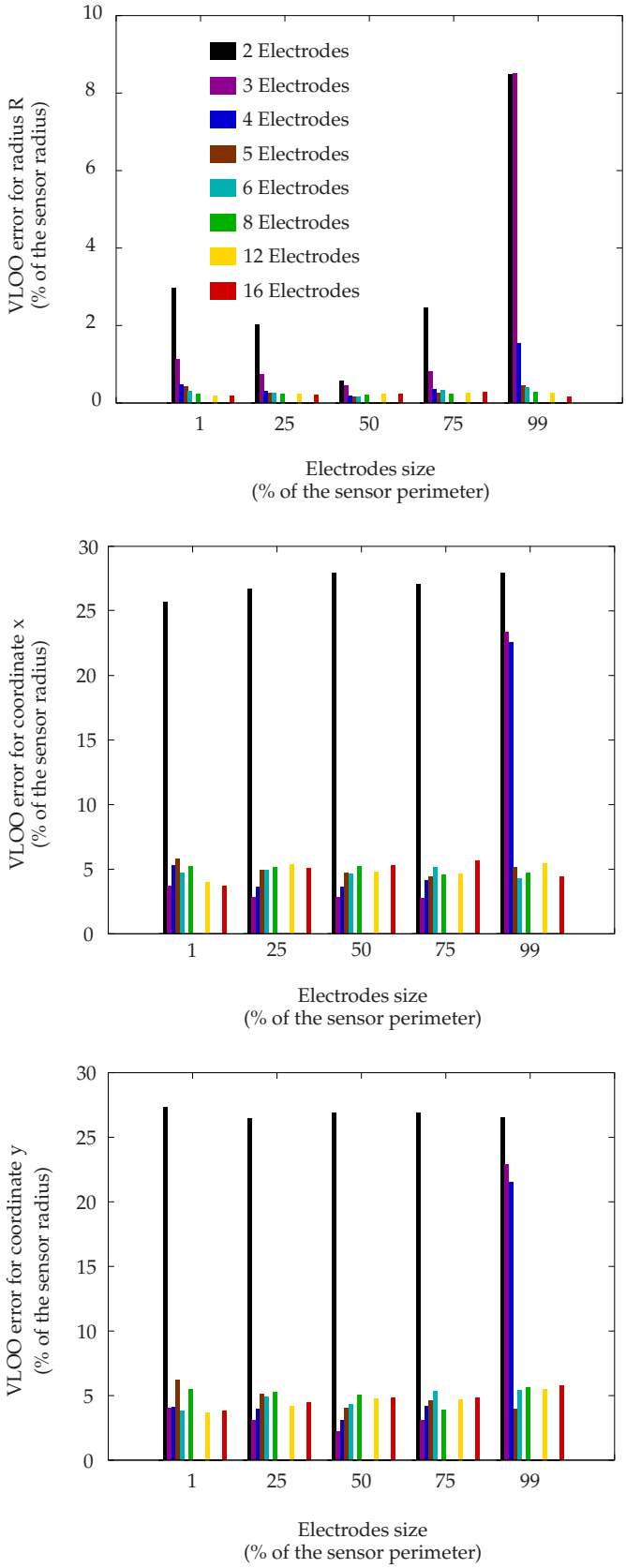

Figure 5: VLOO error for predicting radius R (top), coordinate x (center) and coordinate y (bottom) in a fixed permittivity environment of $\varepsilon_2 = 1$.

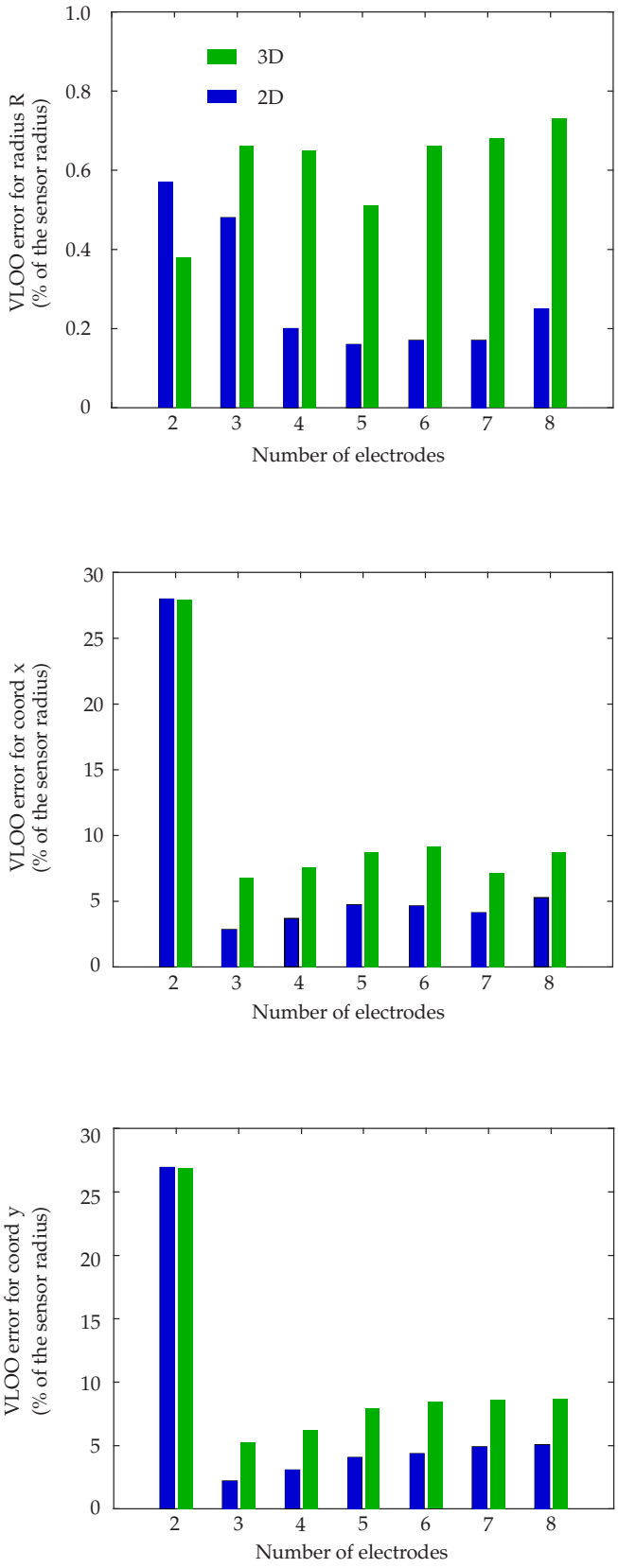

Figure 6: VLOO error for predicting radius R (top), coordinate x (center) and coordinate y (bottom) with both 2D and 3D simulations with intermediate size electrodes of 50%.

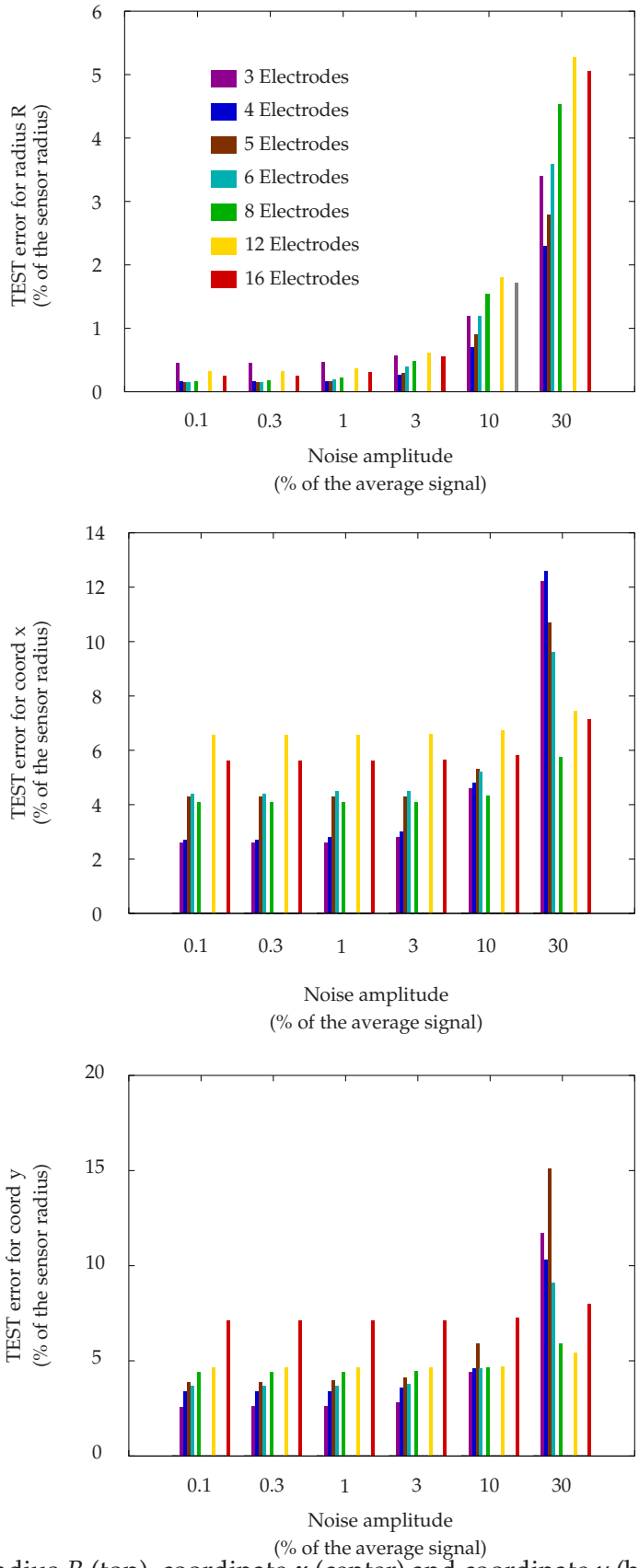

Figure 7: Test error for radius R (top), coordinate x (center) and coordinate y (bottom) with noisy measurements.

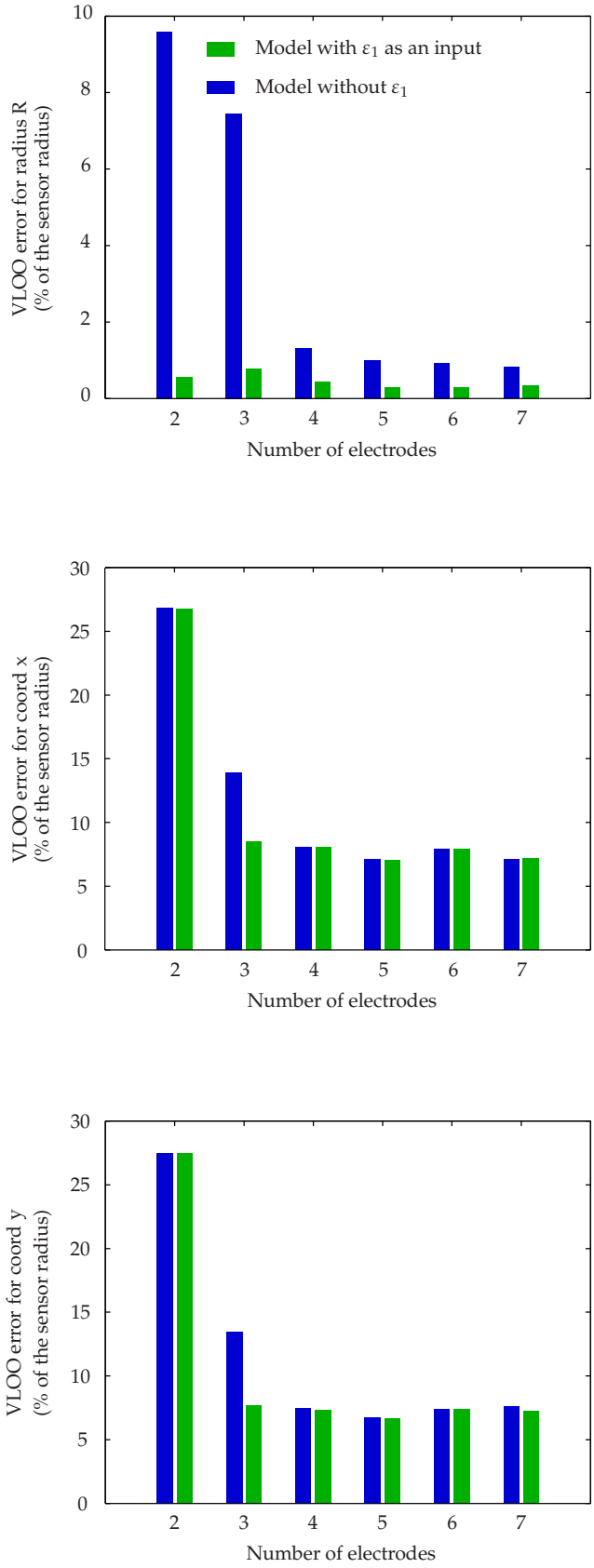

Figure 8: VLOO error for predicting radius R (top), coordinate x (center) and coordinate y (bottom) in a variable permittivity environment.